

Single-stage gradient-based stellarator coil design: stochastic optimization

Florian Wechsung¹, Andrew Giuliani¹, Matt Landreman²,
Antoine Cerfon¹, Georg Stadler¹

¹ Courant Institute of Mathematical Sciences, New York University, New York, USA

² University of Maryland-College Park, Maryland, USA

E-mail: wechsung@nyu.edu, giuliani@cims.nyu.edu, mattland@umd.edu, cerfon@cims.nyu.edu, stadler@cims.nyu.edu

24 June 2021

Abstract. We extend the single-stage stellarator coil design approach for quasi-symmetry on axis from [Giuliani et al, 2020] to additionally take into account coil manufacturing errors. By modeling coil errors independently from the coil discretization, we have the flexibility to consider realistic forms of coil errors. The corresponding stochastic optimization problems are formulated using a risk-neutral approach and risk-averse approaches. We present an efficient, gradient-based descent algorithm which relies on analytical derivatives to solve these problems. In a comprehensive numerical study, we compare the coil designs resulting from deterministic and risk-neutral stochastic optimization and find that the risk-neutral formulation results in more robust configurations and reduces the number of local minima of the optimization problem. We also compare deterministic and risk-neutral approaches in terms of quasi-symmetry on and away from the magnetic axis, and in terms of the confinement of particles released close to the axis. Finally, we show that for the optimization problems we consider, a risk-averse objective using the Conditional Value-at-Risk leads to results which are similar to the risk-neutral objective.

1. Introduction

The design, manufacturing, and assembly of the primary coil system for stellarators are among the most technically challenging aspects of the construction of stellarators [Str+09; Nei+10; Kli+13], and represent a large fraction of the total construction cost. Some of these challenges are intrinsic to the nature of stellarators: non-axisymmetric coil systems are expected to be more complex than the axisymmetric coil systems of tokamaks [Str+09; Gat+18]. However, some of these challenges are directly linked to the design optimization process, and the optima which have been selected for construction. Specifically, the emphasis has historically been given to optimization metrics corresponding to plasma performance, and less attention was given to the engineering requirements and constraints to achieve such performance. Stellarator designs considered optimal from a physics point of view could only be realized with complex and expensive coil configurations. The difficulties encountered in the construction of large scale stellarators [Str+09; Nei+10; Kli+13] has recently

triggered a renewed research effort toward the development of tools enabling the design of simpler and more efficient coil systems that still lead to strong plasma performance [LB16; Lan17; Hud+18; Pau+18; CPD21].

Beside the engineering complexity of a given design, the lack of robustness of the physics performance in the presence of coil manufacturing and assembly errors is also a strong driver for the cost of a machine, since it requires tight tolerances at every step of the manufacturing and assembly process. Both challenges are related but not identical: a relatively simple coil system whose performance degrades strongly with manufacturing and alignment errors may not be as desirable as a more complex coil system with more robust performance. Work has therefore also been lately devoted to the design of efficient numerical methods for the evaluation of the sensitivity of error fields to coil perturbations [Zhu+18b; Zhu+19], and the sensitivity of physical quantities to error fields [LP18; GLP21]. These methods can be included in deterministic stellarator optimization codes, and serve to narrow the search to configurations with lower sensitivity or with sensitivity with respect to perturbations that are more easily controlled.

A complementary approach to deal with the challenge of strong sensitivity and tight tolerances is to account for errors during the optimization process, via stochastic optimization. These errors may either be engineering errors or possibly errors due to the limitations of the physics models used. In stochastic optimization, the objective is a function both of the controls and of the random model errors and hence is itself a random variable. This is precisely the approach we adopt in this article, with the randomness corresponding to perturbations of the location and shape of the coils. We observe that while stochastic optimization is not yet a widely applied method for the design of magnetic confinement devices, it was used in the design of the CNT stellarator [Kre+03; Ped+06]. CNT consists of four circular coils, namely two interlocking (IL) coils and two poloidal field (PF) coils, and the CNT optimization problem involves the angle between the IL coils, as well as the current ratio between the IL and the PF coils. Coil errors involving tilts and shifts of these coils were considered and the goal was to optimize the average volume with good flux surfaces. More recently, for the problem of designing coils corresponding to a desired plasma boundary, Lobsien *et al.* [Lob+20b; Lob+20a] demonstrated that stochastic optimization leads to simpler and better performing coils.

In this manuscript we present a stochastic version of the single-stage coil design framework recently introduced in [Giu+20]. As the purpose of our work is mainly to introduce a new paradigm for stochastic coil design optimization, the physics basis for the design is simple: we consider a vacuum field, and optimize directly for a target value of the rotational transform and for quasi-symmetry on the magnetic axis. The main contribution of this work is a formulation that enables us to consider more general and realistic coil perturbations than considered thus far, to implement gradient based optimisation algorithms relying on analytic derivatives, and to compare the performance of different forms of stochastic optimization.

We find that both the stochastic and deterministic formulations result in different designs depending on the initialization of the optimization algorithm, which indicates the existence of multiple local minima. However, the variability of the designs corresponding to the stochastic problem is substantially reduced as compared to the designs obtained from the deterministic optimization problem. The coil systems we obtain for different initial conditions are much more similar to one another when using stochastic optimization than with deterministic optimization. We compare the

performance of the obtained configurations in the presence of coil errors by evaluating the level of quasi symmetry near and away from the axis, the rotational transform on axis as well as particle loss fraction. We observe that the configurations found by stochastic optimization outperform those obtained from the deterministic formulation. Furthermore, the different minima obtained from stochastic minimization all perform very similarly, which suggests that the optimization algorithm does not get trapped in poor local minima. For all these reasons, our work demonstrates the strong potential of stochastic optimization for stellarator design, and motivates its application to more detailed reactor design studies.

The structure of the article is as follows. In Section 2, we present our mathematical description of the coils, and explain how we model random coil perturbations. In Section 3, we provide a brief summary of stochastic optimization, with a description of several variants which are relevant to stellarator design. We then review in Section 4 the direct coil design paradigm that we modify for stochastic optimization, first introduced in [Giu+20]. We present our main numerical results in Section 5, and summarize our work in Section 6, where we also suggest directions for future work.

2. Modeling coil perturbations

2.1. Physical representation of coil perturbations

For this work, we make the common assumption in coil design that we can represent the coils as current-carrying filaments, i.e., we neglect the non-zero thickness of the coils, and simply model coils as curves in space. A coil is then described by a periodic function $\Gamma : [0, 2\pi) \rightarrow \mathbb{R}^3$. A standard approach to discretizing such coils is given by a truncated Fourier expansion, that is the j -th coordinate of the i -th coil $\Gamma^{(i)}$ is given by

$$\Gamma_j^{(i)}(\theta) = c_{j,0}^{(i)} + \sum_{l=1}^{n_p^{\text{coil}}} s_{j,l}^{(i)} \sin(l\theta) + \sum_{l=1}^{n_p^{\text{coil}}} c_{j,l}^{(i)} \cos(l\theta). \quad (1)$$

We collect the degrees of freedom for coil i in the vector $\mathbf{c}^{(i)} \in \mathbb{R}^{3(2n_p^{\text{coils}}+1)}$. This approach is also used in the FOCUS code [Zhu+18c]. We note that this formulation allows the coils to move freely in space, as compared to coil optimization codes that restrict the coils to lie on the so-called *winding surface*. This latter approach is employed in the ONSET [Dre99], COILOPT [SBH02], COILOPT++ [Gat+17] codes.

A straightforward way of modelling errors is to perturb the vector containing the degrees of freedom, $\tilde{\mathbf{c}}^{(i)} = \mathbf{c}^{(i)} + \boldsymbol{\varepsilon}$ where $\boldsymbol{\varepsilon}$ is a vector of independent random variables. In the context of coil optimization, this approach has been used in [Lob+18; Lob+20b; Lob+20a] which builds on ONSET and uses splines to represent coils. There the spline anchor points were perturbed by independent, centered Gaussian random variables with small variance. This approach does not require any modification of the objective function implementation and hence a deterministic code can be extended towards stochastic optimization with little effort.

However, coil errors originate from the manufacturing process and are thus independent of the coil description used in the design process. Thus, it is unlikely that manufacturing errors satisfy stellarator symmetry [DH98], a property that most optimization studies and coil design codes assume for simplicity [Dre+13; Zhu+18c; Bad+19; Hen+19]. Hence, using the same parametrization for coil errors as used for

the coils lacks generality, and may be unphysical. For instance, when Fourier modes are used for coils *and* coil errors, these errors affect coils globally and repeat themselves along the coils, with more repetitions with increasing Fourier mode numbers. Using splines to describe the coil geometry as well as manufacturing errors has the advantage of allowing the description of local manufacturing errors. However, if the number of spline anchor points changes, the characteristics of the manufacturing error changes as well. Thus, when the description of the coils and the errors is the same, changing the coil discretization also means changing the type of errors considered and convergence to a limit when refining the coil description is unclear.

For this reason, we separate the discretization of the coils and the modelling of perturbations by considering additive perturbations modelled by Gaussian processes [RW06b]. To the best of our knowledge, this is a novel approach for stellarator coil optimization applications. However, similar approaches have been used in other areas. For instance, such an approach has been used in the context of airfoil optimization in two dimensions [CC11; Wan+11; Liu+17].

2.2. Randomly perturbed coils via stochastic processes

We model the perturbations of the coil by random, periodic functions $\Xi : [0, 2\pi) \rightarrow \mathbb{R}^3$, and denote the perturbed coil by $\tilde{\Gamma}(\theta) = \Gamma(\theta) + \Xi(\theta)$. We choose to model the components (Ξ_1, Ξ_2, Ξ_3) of Ξ as centered Gaussian processes.

We briefly recall the definition and some basic properties of Gaussian processes. A random function Ξ is a centered Gaussian process if for any fixed set $\{\theta_1, \dots, \theta_n\}$ the random vector $(\Xi(\theta_1), \dots, \Xi(\theta_n))$ follows a multi-variate normal distribution with mean zero. The function $C(\theta, \theta') = \text{Cov}(\Xi(\theta), \Xi(\theta'))$ is referred to as the covariance function. Sampling a Gaussian process at points $\{\theta_1, \dots, \theta_n\}$ is then as straightforward as drawing a Gaussian vector with mean zero and covariance matrix $\{C(\theta_i, \theta_j)\}_{i,j}$.

In this work, we make the common assumption that the covariance is stationary, i.e., it is only a function of $\theta - \theta'$. Thus, one can write $C(\theta, \theta') = k(\theta - \theta')$ for some function k . The regularity of the random functions Ξ is directly linked to the regularity of k ; in this work we consider a classical squared exponential covariance function,

$$k(d) = \sigma^2 \exp\left(-\frac{d^2}{2l^2}\right), \quad (2)$$

which results in rather smooth perturbations. Here $\sigma > 0$ controls the overall magnitude of the perturbations, and $l > 0$ is a measure for its length scale. For our problem, we cannot use the covariance function k directly, because we need to guarantee periodicity of Ξ . To address this minor difficulty, we rely on the fact that any covariance function k can be made periodic on $[0, 2\pi)$ by defining

$$\tilde{k}(d) = \sum_{j \in \mathbb{Z}} k(d + j2\pi), \quad (3)$$

see [SS02, (4.42)]. We thus use \tilde{k} instead of k for our optimization studies. For our construction of \tilde{k} , we truncate the sum (3) after just a few terms, since k has exponential decay.

Finally, since our optimization algorithms require the knowledge of derivatives, an additional property of Gaussian processes is relevant to our work. By linearity

(see [RW06a, §9.4], [Adl10, §2.2]) the derivatives of Ξ are also Gaussian and satisfy, for $\theta, \bar{\theta}$:

$$\begin{aligned} \text{Cov}(\Xi'(\theta), \Xi(\bar{\theta})) &= \partial_{\theta} C(\theta, \bar{\theta}) = \tilde{k}'(\theta - \bar{\theta}) \\ \text{Cov}(\Xi(\theta), \Xi'(\bar{\theta})) &= \partial_{\bar{\theta}} C(\theta, \bar{\theta}) = -\tilde{k}'(\theta - \bar{\theta}) \\ \text{Cov}(\Xi'(\theta), \Xi'(\bar{\theta})) &= \partial_{\theta} \partial_{\bar{\theta}} C(\theta, \bar{\theta}) = -\tilde{k}''(\theta - \bar{\theta}), \end{aligned} \quad (4)$$

where the prime denotes derivative with respect to its argument. Thus, we can draw samples $\{\Xi(\theta_1), \dots, \Xi(\theta_n), \Xi'(\theta_1), \dots, \Xi'(\theta_n)\}$ by drawing a Gaussian vector with covariance matrix

$$\Sigma = \begin{bmatrix} \tilde{k}(\theta_1 - \theta_1) & \dots & \tilde{k}(\theta_1 - \theta_n) & -\tilde{k}'(\theta_1 - \theta_1) & \dots & -\tilde{k}'(\theta_1 - \theta_n) \\ \vdots & \ddots & \vdots & \vdots & \ddots & \vdots \\ \tilde{k}(\theta_n - \theta_1) & \dots & \tilde{k}(\theta_n - \theta_n) & -\tilde{k}'(\theta_n - \theta_1) & \dots & -\tilde{k}'(\theta_n - \theta_n) \\ \tilde{k}'(\theta_1 - \theta_1) & \dots & \tilde{k}'(\theta_1 - \theta_n) & -\tilde{k}''(\theta_1 - \theta_1) & \dots & -\tilde{k}''(\theta_1 - \theta_n) \\ \vdots & \ddots & \vdots & \vdots & \ddots & \vdots \\ \tilde{k}'(\theta_n - \theta_1) & \dots & \tilde{k}'(\theta_n - \theta_n) & -\tilde{k}''(\theta_n - \theta_1) & \dots & -\tilde{k}''(\theta_n - \theta_n) \end{bmatrix}. \quad (5)$$

The standard approach to drawing such samples is to compute a matrix square root $\Sigma = LL^T$ (e.g. via a Cholesky decomposition) and to draw a standard Gaussian vector \mathbf{z} . It is then straightforward to check that $\text{Cov}(L\mathbf{z}) = \Sigma$. We show several random function draws from this Gaussian process as well as a perturbed coil in Figure 1.

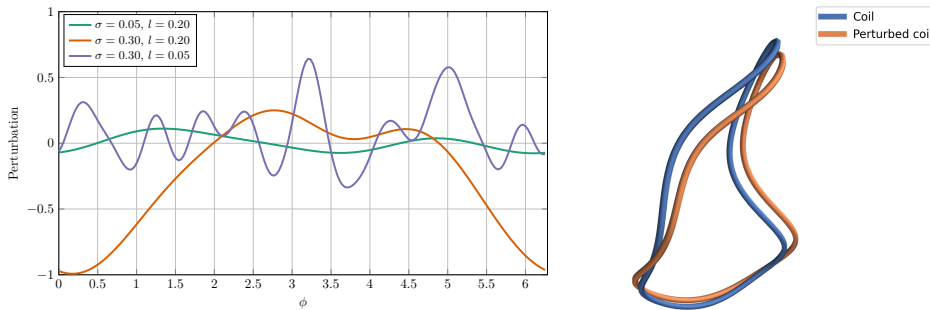


Figure 1. Left: examples of periodic Gaussian processes for different parameter choices σ and l in (2). Right: a coil perturbed with a Gaussian process sample corresponding to $\sigma = 0.1, l = 0.2$. This large value of σ has been chosen for illustration purposes. In our design process we choose smaller σ modeling realistic manufacturing errors.

3. Stochastic and risk-averse optimization

In this Section, we briefly review the mathematical formulations of the different forms of stochastic optimization one may favour, depending on the coil optimization design goals and the level of risk one is willing to tolerate.

Let $f(\{\Gamma^{(i)}\}_{i=1}^{n_c}, \mathbf{q})$ be some quantity of interest which one wants to minimize, and which depends on the coil geometry $\{\Gamma^{(i)}\}_{i=1}^{n_c}$, as well as other quantities $\mathbf{q} \in \mathbb{R}^{n_q}$ (e.g. coil currents). We define

$$g(\{\{\Gamma^{(i)}\}_{i=1}^{n_c}, \mathbf{q}\}, \{\Xi^{(i)}\}_{i=1}^{n_c}) = f(\{\{\Gamma^{(i)} + \Xi^{(i)}\}_{i=1}^{n_c}, \mathbf{q}\}) \quad (6)$$

For notational brevity we write $\mathbf{x} = (\{\mathbf{\Gamma}^{(i)}\}_{i=1}^{n_c}, \mathbf{q})$ and $\zeta = \{\Xi^{(i)}\}_{i=1}^{n_c}$, i.e., the variables to be optimized are contained in \mathbf{x} and the randomness is contained in ζ . For fixed \mathbf{x} , $g(\mathbf{x}, \zeta)$ is now a random variable, which needs to be scalarized in order to perform optimization. Risk-neutral, risk-averse, and robust stochastic optimization formulations are all obtained by different ways of scalarising $g(\mathbf{x}, \zeta)$, and thus all take the distribution of manufacturing errors into account. While other stochastic optimization formulations exist (e.g., [SDR09]), we only describe these three below, since they are the most common formulations, and well suited to stellarator optimization.

Before we do so, we observe that the deterministic optimization problem of minimizing f is equivalent to minimizing

$$\min_{\mathbf{x}} g(\mathbf{x}, 0), \quad (7)$$

i.e., it is assumed that no coil error is present. This is the approach traditionally taken in stellarator optimization, sometimes followed by perturbation tests at the optimal design [Rum+04; Zhu+18c; Zhu+18a; Giu+20] to evaluate the sensitivity of the objective with respect to coil errors. In contrast, the approaches discussed next take the distribution of manufacturing errors into account *during* the optimization process.

3.1. Types of optimization under uncertainty

3.1.1. Risk-neutral stochastic optimization Risk-neutral stochastic optimization corresponds to the situation in which one wants to find a solution \mathbf{x} that performs optimally with respect to the mean of the realisations. We thus obtain the optimization problem

$$\min_{\mathbf{x}} \mathbb{E} [g(\mathbf{x}, \zeta)], \quad (8)$$

where $\mathbb{E}[\cdot]$ denotes expectation over the distribution of the perturbations ζ . In this article, we will mainly focus on this approach, and thus sometimes simply refer to it as *stochastic optimization*. However, for certain stellarator design problems and certain objective functions, it can be desirable to explicitly avoid poor objective values for some realizations of ζ . This can be achieved using risk-averse or robust formulations, which we summarize next.

3.1.2. Risk-averse stochastic optimization: CVaR A measure that focuses on the tail of the distribution is the conditional value-at-risk, or CVaR. The CVaR of a random variable Z is defined as the expected value given that the random variable falls into the α -quantile of its distribution, i.e.,

$$\text{CVaR}_\alpha [Z] = \mathbb{E} [Z | Z > \text{CDF}_Z^{-1}(\alpha)], \quad (9)$$

where CDF_Z denotes the cumulative distribution function and $\alpha \in [0, 1]$. The difference between the risk-neutral formulation and CVaR is illustrated with an example probability density function in Figure 2. This example highlights the fact that the CVaR only depends on the tail of the distribution. One reason for the popularity of CVaR over other risk-averse measures is its convexity as well as the following equivalent formulation (cf. [RU00, Theorem 1])

$$\text{CVaR}_\alpha [Z] = \inf_{t \in \mathbb{R}} \left[t + \frac{1}{1 - \alpha} \mathbb{E} [(Z - t)^+] \right], \quad (10)$$

where $s^+ := \max(0, s)$, which is a convenient formulation for computational purposes. To cope with the non-differentiable nature of the max-function, one relies in practice on a smooth approximation $h_\varepsilon : \mathbb{R} \rightarrow [0, \infty)$ with $h_\varepsilon \rightarrow (\cdot)^+$ as $\varepsilon \rightarrow 0$. The specific form of h_ε used in this work is

$$h_\varepsilon(x) = \begin{cases} x & \text{if } x \geq \varepsilon/2, \\ \frac{(x+\varepsilon/2)^3}{\varepsilon^2} - \frac{(x+\varepsilon/2)^4}{2\varepsilon^3} & \text{if } -\varepsilon/2 < x < \varepsilon/2, \\ 0 & \text{otherwise.} \end{cases} \quad (11)$$

We thus obtain the optimization problem

$$\min_{\mathbf{x}, t} \left[t + \frac{1}{1-\alpha} \mathbb{E} [h_\varepsilon(g(\mathbf{x}, \zeta) - t)] \right] \quad (12)$$

for a small ε . Risk-averse formulations based on CVaR are successfully used in the insurance and finance industries and in engineering [RU00; KPU02; KS16] for instance.

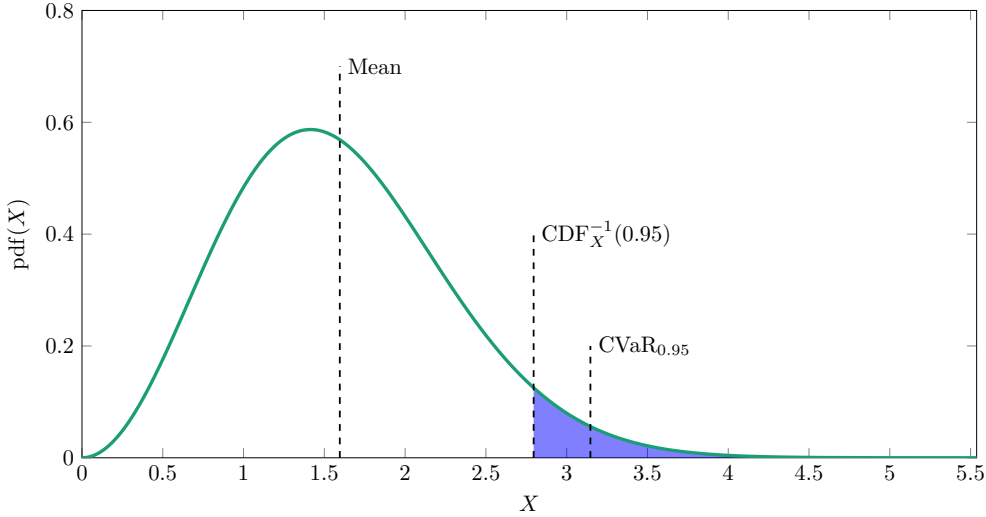


Figure 2. Illustration of mean and CVaR with $\alpha = 0.95$ for an example distribution whose probability density function is shown in green.

3.1.3. Robust stochastic optimization To completely control the probability of poor outcomes, one can optimize the worst possible scenario, i.e.,

$$\min_{\mathbf{x}} \max_{\zeta} g(\mathbf{x}, \zeta). \quad (13)$$

This formulation is typically combined with a model for randomness that results in perturbations that are almost surely bounded. We will observe in Section 5 that the difference between risk-neutral and risk-averse coil designs is minor for the stellarator optimization problem we consider. Thus, we do not explore robust optimization further in this article, as it can be viewed as an extreme version of risk-averse optimization.

3.2. Sample average approximation

The expected value in (8) and (12) can typically not be computed analytically but has to be approximated numerically. For that purpose, we use the *sample average approximation*, i.e., we draw N_{MC} independent realisations of ζ_k and approximate

$$\begin{aligned}\mathbb{E}[g(\mathbf{x}, \zeta)] &\approx \frac{1}{N_{\text{MC}}} \sum_{k=1}^{N_{\text{MC}}} g(\mathbf{x}, \zeta_k), \\ \mathbb{E}[h_\varepsilon(g(\mathbf{x}, \zeta) - t)] &\approx \frac{1}{N_{\text{MC}}} \sum_{k=1}^{N_{\text{MC}}} h_\varepsilon(g(\mathbf{x}, \zeta_k) - t),\end{aligned}\tag{14}$$

for the risk-neutral and risk-averse formulation respectively. As $N_{\text{MC}} \rightarrow \infty$, the random space approximation error is of the typical Monte Carlo order $O(N_{\text{MC}}^{-1/2})$. Since the samples ζ_k are kept fixed throughout the optimization, (14) results in a deterministic optimization problem with N_{MC} terms. Note that by linearity the sample average approximation of the gradients is exactly equal to the gradient of the sample average approximation.

Our numerical tests in Section 5 focus on a comparison between deterministic, risk-neutral and CVaR risk-averse stochastic designs. Moreover, we study the role of the Monte Carlo sample size N_{MC} for approximating the distribution.

4. Direct coil design for quasi-symmetry in vacuum fields

In [Giu+20] a new formulation was presented to directly design coils generating vacuum magnetic fields which are quasi-symmetric to high accuracy in a region close to the magnetic axis. We briefly recall the basic structure of the objective that was developed there and then show the corresponding stochastic and risk-averse formulations.

Given a so-called expansion axis $\Gamma_{\mathbf{a}}$ and real parameter $\bar{\eta}$ it was shown in [LS18; LSP19] how to construct a magnetic field \mathbf{B}_{QS} that is quasi-symmetric near the axis and how to compute its rotational transform ι . Calling $\mathbf{B}_{\text{coils}}$ the magnetic fields induced by the coils $\{\Gamma_{\mathbf{c}}^{(i)}\}$, the approach of [Giu+20] is then to find coils so that $\mathbf{B}_{QS} \approx \mathbf{B}_{\text{coils}}$. Grouping the coefficients that describe the expansion axis and the real parameter η in a vector \mathbf{a} , and grouping the coefficients that describe the coils and their currents in a vector \mathbf{c} , the objective is given by

$$\begin{aligned}\hat{J}(\mathbf{c}, \mathbf{a}) &= \frac{1}{2} \int_{\Gamma_{\mathbf{a}}} \|\mathbf{B}_{\text{coils}}(\mathbf{c}) - \mathbf{B}_{QS}(\mathbf{a})\|^2 dl + \frac{1}{2} \int_{\Gamma_{\mathbf{a}}} \|\nabla \mathbf{B}_{\text{coils}}(\mathbf{c}) - \nabla \mathbf{B}_{QS}(\mathbf{a})\|^2 dl \\ &\quad + \frac{1}{2} \left(\frac{(\iota(\mathbf{a}) - \iota_{0,a})^2}{\iota_{0,a}^2} \right) + R_a(\mathbf{a}) + R_c(\mathbf{c}),\end{aligned}\tag{15}$$

where $\iota_{0,a}$ is a target rotational transform, and R_a and R_c contain various regularizations for the expansion axis and coils respectively. The regularization terms include penalty functions for the length of the axis and the length of the coils, the curvature of the coils, and the distance between coils. In [Giu+20] it was shown that this formulation leads to an efficient method to design *from scratch* coils producing nearly quasi-symmetric vacuum magnetic configurations, and to improve the quasi-symmetry properties of existing designs.

Random perturbations of the coils can be taken into account by considering the objective

$$\begin{aligned} \hat{J}(\mathbf{c}, \mathbf{a}, \boldsymbol{\zeta}) &= \frac{1}{2} \int_{\Gamma_{\mathbf{a}}} \|\mathbf{B}_{\text{coils}}(\mathbf{c}, \boldsymbol{\zeta}) - \mathbf{B}_{\text{QS}}(\mathbf{a})\|^2 dl + \frac{1}{2} \int_{\Gamma_{\mathbf{a}}} \|\nabla \mathbf{B}_{\text{coils}}(\mathbf{c}, \boldsymbol{\zeta}) - \nabla \mathbf{B}_{\text{QS}}(\mathbf{a})\|^2 dl \\ &\quad + \frac{1}{2} \left(\frac{(l - l_{0,a})^2}{l_{0,a}^2} \right) + R_a(\mathbf{a}) + R_c(\mathbf{c}), \end{aligned} \tag{16}$$

where $\mathbf{B}_{\text{coils}}(\mathbf{c}, \boldsymbol{\zeta})$ corresponds to the magnetic field produced by the perturbed coils $\{\boldsymbol{\Gamma}^{(i)} + \boldsymbol{\Xi}^{(i)}\}$. We emphasize here that the field \mathbf{B}_{QS} and the rotational transform are independent from the random variable $\boldsymbol{\zeta}$, and hence we only have to recompute $\mathbf{B}_{\text{coils}}(\mathbf{c}, \boldsymbol{\zeta})$ and $\nabla \mathbf{B}_{\text{coils}}(\mathbf{c}, \boldsymbol{\zeta})$ for different samples $\boldsymbol{\zeta}$. We observe that as it is stated here, the optimization problem can lead to numerical difficulties, because vanishing derivatives of $\boldsymbol{\Gamma}^{(i)}$ result in a non differentiable curve length objective, and because of the large nullspace of the objective, which is partially due to the fact that different parametrizations give the same physical curve. In order to address these numerical difficulties, we add the following regularization term, in addition to the axis length, coil length, coil curvature, and coil distance terms already included in [Giu+20],

$$R_{\text{arc}}(\mathbf{c}) = \sum_{i=1}^{n_c} \int_{[0, 2\pi)} (\|\boldsymbol{\Gamma}^{(i)'}(\theta)\| - t^{(i)})^2 d\theta, \tag{17}$$

where $t^{(i)} = \frac{l^i}{2\pi}$ is the value that would correspond to a constant-arclength parametrization of a circle with coil length $l^{(i)}$.

5. Numerical results for NCSX-like example

5.1. Implementation and setup

We implement this optimization in the open source PyPlasmaOpt package available under <https://github.com/florianwechsung/PyPlasmaOpt>. PyPlasmaOpt is a Python library that relies on the geometric objects and the Biot Savart implementation of the SIMSOPT stellarator optimization package <http://github.com/hiddenSymmetries/SIMSOPT>. The implementation is parallelized across samples using MPI, and the Biot Savart computation is accelerated using SIMD instructions as well as OpenMP. A function and gradient evaluation of a typical configuration (18 coils, 120 quadrature points per coil) with 1024 samples takes less than half of a second on a machine with two 24 Core Intel Xeon Platinum 8268 processors.

To solve the optimization problems in (7), (8), and (12), we use the L-BFGS implementation in SciPy [Vir+20]. For the smoothed risk-averse objective, we use the risk-neutral minimizer as initial guess, then solve the optimization problem, then reduce the smoothing parameter ε , and then solve the problem again, using the previous solution as initial guess. This is repeated until $\varepsilon = 10^{-5}$.

We study a configuration that is inspired by the National Compact stellarator Experiment (NCSX). NCSX consists of three distinct modular coils, which results in 18 coils after applying three fold rotational symmetry and stellarator symmetry. We re-emphasize that while the design space only consists of coils that satisfy these symmetries, the perturbations are not required to satisfy any form of symmetry. For full details of the configuration we refer to [Giu+20, Section 6]. Finally, we note that

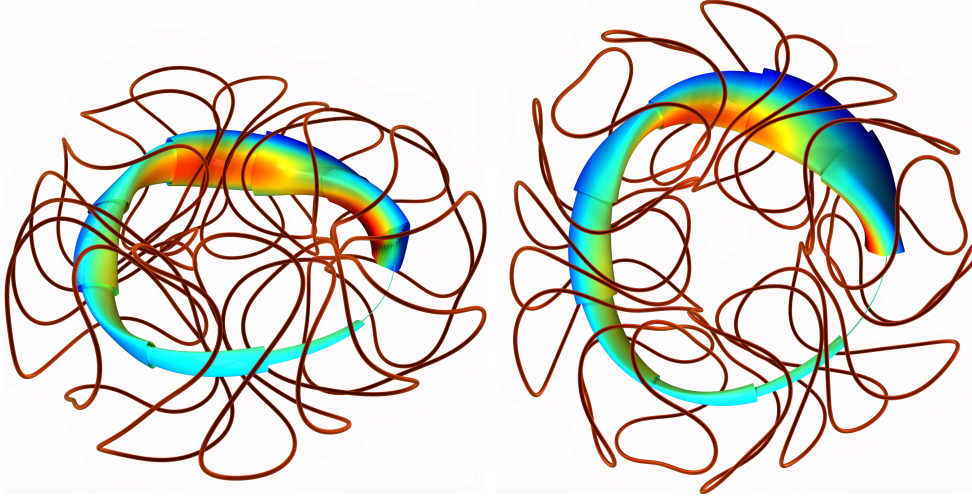


Figure 3. Two views of an optimal stellarator design computed using risk-neutral stochastic optimization with $N_{MC} = 1024$ samples with $\sigma = 10^{-2}$. We also show a range of nested magnetic surfaces, with cool colors corresponding to low field strength and warm colors corresponding to high field strength.

NCSX was designed for finite pressure equilibria, as opposed to the vacuum field that we consider here, and that the additional planar coils of the NCSX design are ignored in our calculations.

We study this problem in particular as the NCSX project was cancelled due to increasing costs because of, among other reasons, the requirement of tight engineering tolerances on the coils. To model the distribution of manufacturing errors, we choose a length scale of $l = 0.4\pi$ and a standard deviations of either $\sigma = 10^{-2}$ or $\sigma = 3 \times 10^{-3}$ in the kernel (2) defining the Gaussian process. For each of the coils, these values correspond to manufacturing errors of a few centimeters for $\sigma = 10^{-2}$ and several millimeters for $\sigma = 3 \times 10^{-3}$.

When running the optimization algorithm with different initial guesses, we observe that multiple local minima exist. For this reason, in the following sections we usually show results for several different minima, that were obtained by starting the optimizer from eight different initial guesses. These initial guesses were obtained by randomly perturbing the Fourier coefficients describing the coils using independent normal random variables with standard deviation of 0.01. One of the obtained configurations together with a range of magnetic surfaces is shown in Figure 3. Next, in Sections 5.2 and 5.3 we mainly focus on the role the number of samples N_{MC} in the sample average approximation (14) plays in approximating the distribution of coil perturbations, and on the sensitivity of both the deterministic and the stochastic minimizers on the initial guesses for the optimization algorithm.

5.2. Deterministic versus stochastic designs

Figure 4 shows minimizers that were obtained by solving the deterministic and the stochastic optimization problem for eight different initial guesses. We clearly see that for the deterministic problem there exists a large number of different minimizers that

are all distinct from each other. As coil errors (with $\sigma = 10^{-2}$) are introduced and the sample average approximation size N_{MC} (see (14)) is increased, the number of distinct minimizers that the algorithm finds is reduced and there is less variation between the different coil designs. We note that the gradient was reduced by over 10 orders of magnitude for all of these minimizers, so we can be confident that this result is not an artifact of a possibly incomplete convergence of the algorithm. It is remarkable that stochastic design formulations are significantly less prone to having multiple minima. Intuitively, this can be understood by the fact that stochastic designs must perform well on average for a distribution of manufacturing errors, which prevents overfitting and also makes the objective locally convex in most directions around a minimizer. In the following discussion, we find several additional advantages that designs computed from a stochastic formulation have compared to designs based on a deterministic formulation.

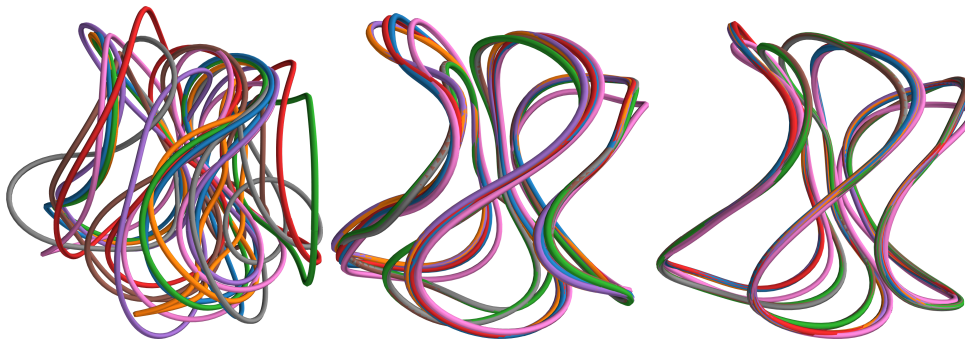


Figure 4. Optimal coil designs for the three independent coils. The designs are obtained by using deterministic optimization (left), risk-neutral stochastic optimization with $N_{\text{MC}} = 4$ samples (middle) and with $N_{\text{MC}} = 1024$ samples (right) for eight different initial guesses (i.e., each panel shows 24 coil shapes). Different colors correspond to different minimizers.

5.3. Out of sample distribution at the minimizer

As we only optimized the mean of the objective for a finite number of perturbations, we have to check that this performance generalises to the full distribution of coil errors. To do this we draw a large number (2^{18}) of new samples, which are different from those used in the sample average approximation, and evaluate the objective at the minimizer for each of the samples. In the context of statistics and machine learning, this procedure is known as out-of-sample testing or cross validation. Figure 5 shows the resulting distribution for minimizers obtained from deterministic and stochastic optimization from eight different initial guesses. We see that the performance of the minimizers of the deterministic optimization problem varies strongly on perturbed coils. The minimizers found by stochastic optimization have lower objective value on average and for most perturbations. In other words, the stochastic designs perform significantly better than the deterministic designs. Additionally, different minimizers obtained as a result of different initializations of the algorithm perform vastly differently for the deterministic formulation, but very similarly for the stochastic formulations, in particular when 1024 samples are used to estimate the expected value in (14) for the stochastic formulation.

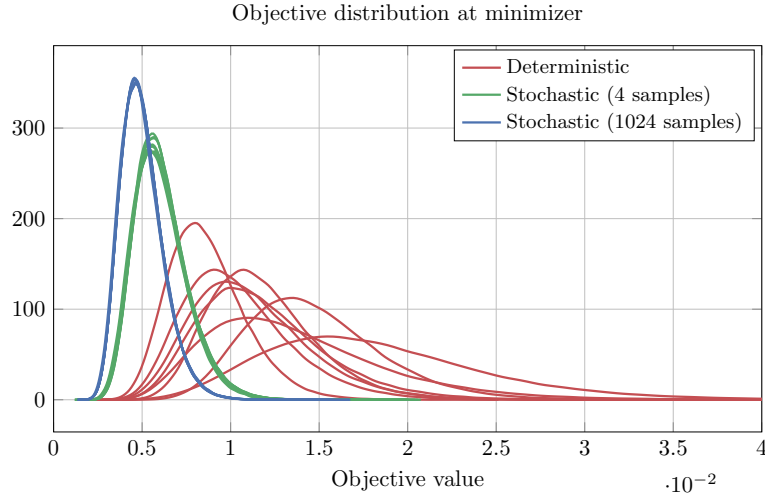


Figure 5. Kernel density estimate for the distribution of the objective value evaluated at minimizers obtained by running deterministic (red) and stochastic optimization with $N_{MC} = 4$ and $N_{MC} = 1024$ samples used in the sample average approximation (green and blue, respectively). Eight different initial guesses are used for each optimization, leading to different minimizers and thus different distributions. The distribution is approximated using $2^{18} = 262,144$ independent samples drawn from the error distribution.

5.4. Quasi-symmetry close to the axis

The objective is designed to ensure quasi-symmetry near the axis. To confirm that this is achieved and to investigate the magnetic field away from the axis, we compute magnetic flux surfaces $\mathbf{S}(\varphi, \theta)$ parametrized by Boozer angles φ and θ . We recall that a magnetic field is called quasi-axisymmetric if $|\mathbf{B}(\mathbf{S}(\varphi, \theta))|$ is a function of θ only. Figure 6 shows three surfaces computed for the best configuration obtained from stochastic optimization with $N_{MC} = 1024$ samples. We can see that for the surface closest to the axis, the field strength is indeed close to constant in φ . As we move away from the axis, this property is gradually lost.

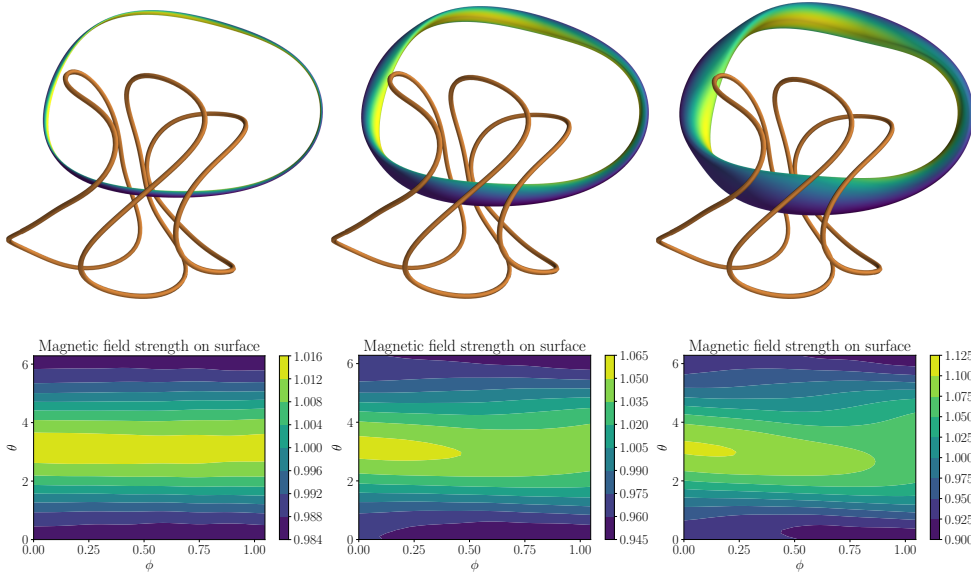


Figure 6. Top: Coils and magnetic surfaces in Boozer coordinates for the best configuration obtained from stochastic optimization with $N_{MC} = 1024$ samples. Bottom: Strength of the magnetic field as a function of Boozer angles φ and θ on the surfaces shown on the top. Perfect quasi-symmetry corresponds to the magnetic field strength being independent of φ .

To quantify this statement, we decompose $|\mathbf{B}|$ into a quasi-symmetric and non-quasi-symmetric part by defining

$$\|\mathbf{B}\|_{QS}(\theta) = \frac{\int_{[0,2\pi)} \|\mathbf{B}(\mathbf{S}(\varphi, \theta))\| \|\partial_\varphi \mathbf{S} \times \partial_\theta \mathbf{S}\| d\varphi}{\int_{[0,2\pi)} \|\partial_\varphi \mathbf{S} \times \partial_\theta \mathbf{S}\| d\varphi}$$

$$\|\mathbf{B}\|_{NotQS}(\varphi, \theta) = \|\mathbf{B}(\mathbf{S}(\varphi, \theta))\| - \|\mathbf{B}\|_{QS}(\theta).$$

We then measure the norm of the non-quasi-symmetric part and report $\left[\frac{\iint_{\mathbf{S}} \|\mathbf{B}\|_{NotQS}^2 dS}{\iint_{\mathbf{S}} \|\mathbf{B}\|_{QS}^2 dS} \right]^{1/2}$ in Figure 7. Since we only enforce quasi-symmetry near the axis, we expect this measure to be small for surfaces close to the axis, and to increase as we move away from the axis.

We perform the stochastic optimization for $\sigma_{opt} = 0.01$ and $\sigma_{opt} = 0.003$. Quasi-symmetry is then evaluated by drawing 20 new samples with standard deviation σ_s and computing surfaces for the fields induced by the perturbed coils. The case of $\sigma_s < \sigma_{opt}$ can be viewed as the estimate for the perturbation size in the original optimization being pessimistic, or be due to improvements in the manufacturing process between design and construction of the coils. For comparison, we also compute surface and non-quasi-symmetry for the minimizers obtained from deterministic optimization (corresponding to $\sigma_{opt} = 0$). The results are displayed in Figure 7.

Overall we observe that the configurations have very little non-quasi-symmetric contribution close to the axis, and that the non-quasi-symmetry then increases away from axis. As can be expected, the difference between stochastic and deterministic optimization is most significant for large coil perturbations (left plot, solid lines). Keeping those same configurations, but reducing the perturbation magnitude in the

newly drawn samples, we can see that the configurations obtained from both types of optimization benefit from the added accuracy (left plot, dashed lines). Importantly, the designs from stochastic optimization systematically perform better than those from deterministic optimization.

For smaller perturbations (right) the behaviour remains qualitatively the same, but the overall difference between stochastic and deterministic optimization is smaller. This is expected, as in the limit of $\sigma_{\text{opt}} \rightarrow 0$ the two optimization strategies become identical.

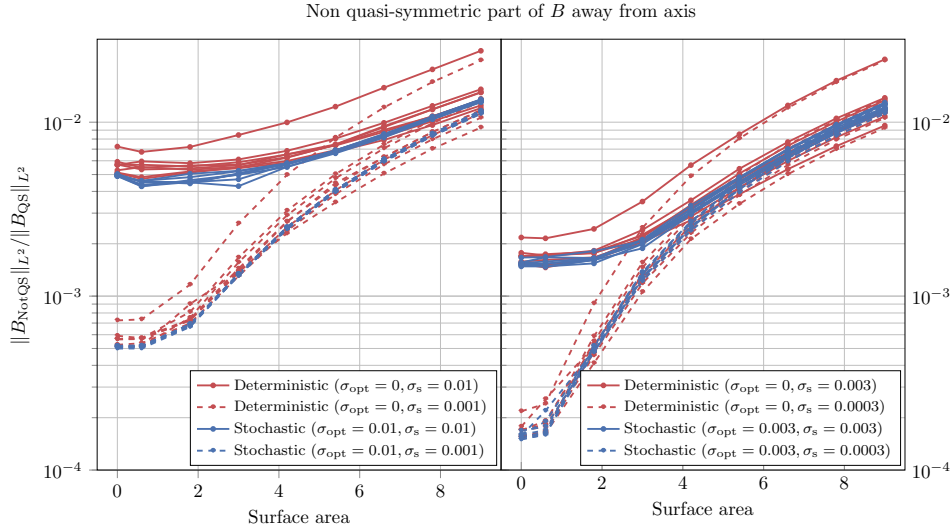


Figure 7. Mean non-quasi-symmetry on a range of surfaces for eight different minimizers obtained from deterministic and stochastic ($N_{\text{MC}} = 1024$ samples) optimization. Here we use the surface area as a label for the surfaces. Larger surface areas correspond to surfaces farther from the axis.

5.5. Rotational transform on axis

The objective includes a penalty that targets a certain rotational transform on the expansion axis. To investigate the impact of coil perturbation errors on rotational transform, we draw 128 sets of perturbed coils, compute the magnetic axis for the resulting magnetic fields, and then compute the rotational transform ι on axis. The resulting distribution of ι is shown in Figure 8. As expected, for the perturbed coils the target rotational transform is not achieved exactly. In agreement with our previous results, we also observe that the different minimizers obtained from deterministic optimization vary more than those obtained from stochastic optimization.

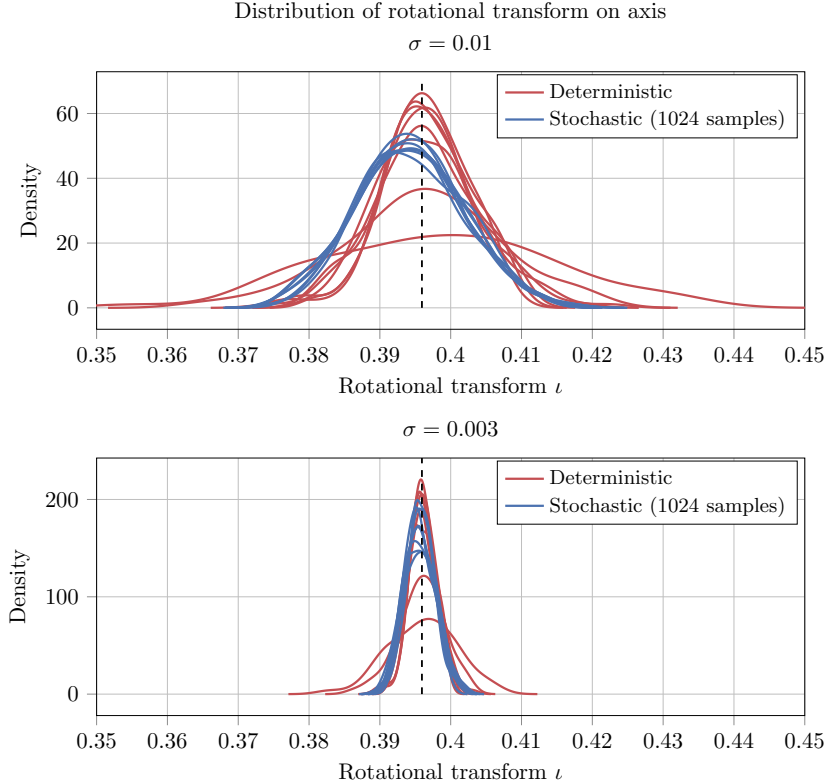


Figure 8. Distribution of the rotational transform ι on axis for each of the eight minimizers found from deterministic and stochastic optimization. The distribution is approximated using 128 independently drawn perturbed coil sets. The dashed line indicated the target rotational transform.

5.6. Particle confinement

As a final measure of performance, we compute particle trajectories for perturbations of the configurations obtained from deterministic and stochastic optimization. We consider both 250eV protons and 1keV protons. For reference, we note that a 3.4keV proton in our designs has approximately the same ratio of gyroradius to machine size as an energetic alpha particle in the ARIES-CS reactor. We draw 10 perturbed coil configurations for each minimizer obtained from deterministic and stochastic optimization, as well as for the initial NCSX-like configuration. We then spawn 1120 protons with random pitch angle on random points along the magnetic axis and follow them for 10ms, using the guiding center approximation [Boo80; Lit83; CB09] without collisions. Particles are considered lost if they move more than 30cm away from the axis. Figure 9 shows the average fraction of lost particles over time.

For both the lower energy protons and the higher energy protons considered here, we observe that the configurations from stochastic optimization have better confinement than the initial configuration and the configurations obtained from deterministic optimization. In addition, we see again that the different minimizers in the stochastic case all perform very similarly, whereas those from deterministic optimization have highly varying performance. For the protons with lower energy,

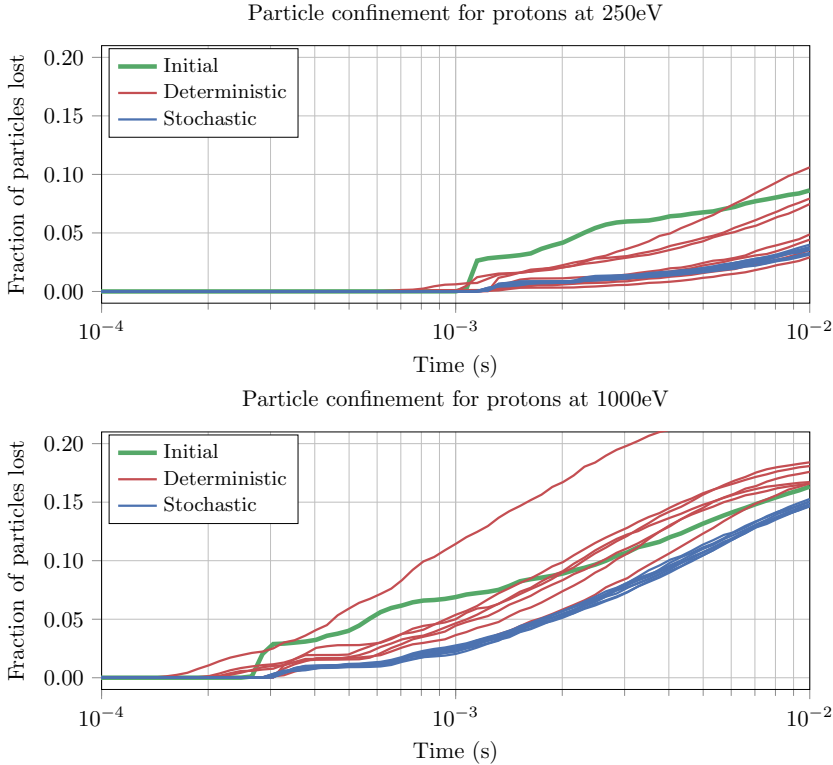


Figure 9. Particle losses over time for 250eV and 1000eV protons spawned on axis, for perturbations of configurations obtained from stochastic and deterministic optimization.

nearly all optimized configurations outperform the initial configuration. However, for the protons with higher energy, this advantage is less clear. This suggests that quasi-symmetry only close to the axis is in general insufficient to guarantee good particle confinement, and motivates ongoing work on direct coil optimization enforcing quasi-symmetry away from the axis.

5.7. Risk-neutral vs. risk-averse optimization

Finally, we compare the risk-neutral formulation (i.e. minimization of the expected value) with a risk-averse objective for an error distribution with $\sigma = 10^{-2}$. We choose $\alpha = 0.95$ and minimize $\text{CVaR}_\alpha(f)$, meaning that we minimize the expected value of the tail containing the 5% worst scenarios. In Figure 10 we show the out-of-sample distribution of the objective evaluated at the minimizers. We can see that most of the distribution for the risk-neutral objective is closer to zero, while the tail is slightly thicker. However, the difference is insignificant. We attribute this to the quadratic penalty form of our objective: since all objective values are positive and the objective is squared, in order to control the mean large positive outliers have to be avoided.

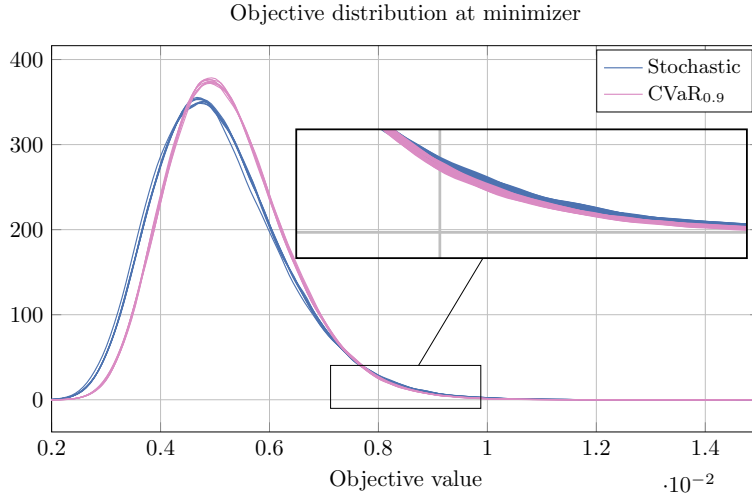


Figure 10. Distribution of objective values for designs computed using risk-neutral stochastic formulation (blue) and CVaR risk-averse stochastic formulation (pink). $N_{MC} = 1024$ samples are used in the stochastic optimization, and the distributions are computed using 262144 independent samples. Slightly different designs are obtained using eight initializations for the optimization.

6. Conclusion and future work

We have extended the direct stellarator design approach of [Giu+20] to include random coil errors. We emphasize that our formulation uses separate discretizations for the coils and their errors, which allows us to retain symmetries in the design space but considers perturbations that do not satisfy them.

We then studied and compared deterministic, risk-neutral, and risk-averse optimization for an NCSX-like example. We found that the deterministic problem admits a large number of distinct minimizers which perform quite differently. Including stochasticity reduces the number of different minimizers and results in minimizers that all perform nearly identical in terms of both objective value, as well as quasi-symmetry and rotational transform on and away from axis. Moving from a risk-neutral to a risk-averse formulation does not result in significantly different minimizing designs in our experiments: the tail of the distribution is reduced at the cost of somewhat worse average performance. Finally, while we are able to achieve quasi-symmetry near the axis, this property is lost away from axis. Current work is focused on including the non-quasi-symmetry measure presented in Figure 7 on a range of surfaces to enforce quasi-symmetry away from axis.

Acknowledgments

This work was supported by a grant from the Simons Foundation (560651). AG is partially supported by a NSERC (Natural Sciences and Engineering Research Council of Canada) postdoctoral fellowship. In addition, this work was supported in part through the NYU IT High Performance Computing resources, services, and staff expertise.

Code availability

The code used to generate the numerical results is openly available under

<https://github.com/florianwechsung/PyPlasmaOpt/tree/fw/paper-stochastic/examples/stochastic>

References

- Adler, Robert J. *The Geometry of Random Fields*. en. Society for Industrial and Applied Mathematics, Jan. 2010. DOI: 10.1137/1.9780898718980.
- Bader, Aaron et al. “Stellarator equilibria with reactor relevant energetic particle losses”. In: *Journal of Plasma Physics* 85.5 (2019), p. 905850508. DOI: 10.1017/S0022377819000680.
- Boozer, Allen H. “Guiding center drift equations”. In: *The Physics of Fluids* 23.5 (1980), pp. 904–908. DOI: 10.1063/1.863080. eprint: <https://aip.scitation.org/doi/pdf/10.1063/1.863080>. URL: <https://aip.scitation.org/doi/abs/10.1063/1.863080>.
- Carlton-Jones, Arthur, Elizabeth J Paul, and William Dorland. “Computing the shape gradient of stellarator coil complexity with respect to the plasma boundary”. In: *Journal of Plasma Physics* 87.2 (2021).
- Cary, John R. and Alain J. Brizard. “Hamiltonian theory of guiding-center motion”. In: *Rev. Mod. Phys.* 81 (2 May 2009), pp. 693–738. DOI: 10.1103/RevModPhys.81.693. URL: <https://link.aps.org/doi/10.1103/RevModPhys.81.693>.
- Chen, Shikui and Wei Chen. “A new level-set based approach to shape and topology optimization under geometric uncertainty”. In: *Structural and Multidisciplinary Optimization* 44.1 (July 2011), pp. 1–18. ISSN: 1615-147X, 1615-1488. DOI: 10.1007/s00158-011-0660-9.
- Dewar, R.L. and S.R. Hudson. “Stellarator symmetry”. In: *Physica D: Nonlinear Phenomena* 112.1 (1998). Proceedings of the Workshop on Time-Reversal Symmetry in Dynamical Systems, pp. 275–280. ISSN: 0167-2789. DOI: [https://doi.org/10.1016/S0167-2789\(97\)00216-9](https://doi.org/10.1016/S0167-2789(97)00216-9).
- Drevlak, M. et al. “ESTELL: A Quasi-Toroidally Symmetric Stellarator”. In: *Contributions to Plasma Physics* 53.6 (2013), pp. 459–468. DOI: 10.1002/ctpp.201200055.
- Drevlak, Michael. “Optimization of heterogenous magnet systems”. In: *Proceedings of the 12th International Stellarator Workshop*. 1999.
- Gates, D.A. et al. “Recent advances in stellarator optimization”. In: *Nuclear Fusion* 57.12 (Dec. 2017), p. 126064. DOI: 10.1088/1741-4326/aa8ba0.
- Gates, David A et al. “Stellarator research opportunities: a report of the National Stellarator Coordinating Committee”. In: *Journal of Fusion Energy* 37.1 (2018), pp. 51–94.
- Geraldini, Alessandro, M. Landreman, and E. Paul. “An adjoint method for determining the sensitivity of island size to magnetic field variations”. In: *Journal of Plasma Physics* 87.3 (2021), p. 905870302. DOI: 10.1017/S0022377821000428.
- Giuliani, Andrew et al. “Single-stage gradient-based stellarator coil design: Optimization for near-axis quasi-symmetry”. In: *arXiv preprint arXiv:2010.02033* (2020).
- Henneberg, S.A. et al. “Properties of a new quasi-axisymmetric configuration”. In: *Nuclear Fusion* 59.2 (2019), p. 026014. DOI: 10.1088/1741-4326/aaf604.

- Hudson, S.R. et al. “Differentiating the shape of stellarator coils with respect to the plasma boundary”. In: *Physics Letters A* 382.38 (2018), pp. 2732–2737. ISSN: 0375-9601. DOI: <https://doi.org/10.1016/j.physleta.2018.07.016>.
- Klinger, T. et al. “Towards assembly completion and preparation of experimental campaigns of Wendelstein 7-X in the perspective of a path to a stellarator fusion power plant”. In: *Fusion Engineering and Design* 88.6 (2013). Proceedings of the 27th Symposium On Fusion Technology (SOFT-27); Liège, Belgium, September 24–28, 2012, pp. 461–465. ISSN: 0920-3796. DOI: <https://doi.org/10.1016/j.fusengdes.2013.02.153>.
- Kouri, D. P. and T. M. Surowiec. “Risk-Averse PDE-Constrained Optimization Using the Conditional Value-At-Risk”. In: *SIAM Journal on Optimization* 26.1 (2016), pp. 365–396. DOI: 10.1137/140954556.
- Kremer, JP et al. “The Status of the Design and Construction of the Columbia Non-neutral Torus”. In: *AIP Conference Proceedings*. Vol. 692. Issue: 1. American Institute of Physics, 2003, pp. 320–325.
- Krokhmal, Pavlo, Jonas Palmquist, and Stanislav Uryasev. “Portfolio optimization with conditional value-at-risk objective and constraints”. In: *Journal of Risk* 4 (2002), pp. 43–68.
- Landreman, Matt. “An improved current potential method for fast computation of stellarator coil shapes”. In: *Nuclear Fusion* 57.4 (Feb. 2017), p. 046003. DOI: 10.1088/1741-4326/aa57d4.
- Landreman, Matt and Allen H. Boozer. “Efficient magnetic fields for supporting toroidal plasmas”. In: *Physics of Plasmas* 23.3 (2016), p. 032506. DOI: 10.1063/1.4943201.
- Landreman, Matt and Elizabeth Paul. “Computing local sensitivity and tolerances for stellarator physics properties using shape gradients”. In: *Nuclear Fusion* 58.7 (June 2018), p. 076023. DOI: 10.1088/1741-4326/aac197. URL: <https://doi.org/10.1088/1741-4326/aac197>.
- Landreman, Matt and Wrick Sengupta. “Direct construction of optimized stellarator shapes. Part 1. Theory in cylindrical coordinates”. In: *Journal of Plasma Physics* 84.6 (2018), p. 905840616. DOI: 10.1017/S0022377818001289.
- Landreman, Matt, Wrick Sengupta, and Gabriel G. Plunk. “Direct construction of optimized stellarator shapes. Part 2. Numerical quasisymmetric solutions”. In: *Journal of Plasma Physics* 85.1 (2019), p. 905850103. DOI: 10.1017/S0022377818001344.
- Littlejohn, R. G. “Variational principles of guiding centre motion”. In: *Journal of Plasma Physics* 29.1 (1983), pp. 111–125. DOI: 10.1017/S002237780000060X.
- Liu, Dishi et al. “Quantification of Airfoil Geometry-Induced Aerodynamic Uncertainties—Comparison of Approaches”. In: *SIAM/ASA Journal on Uncertainty Quantification* 5.1 (Jan. 2017), pp. 334–352. ISSN: 2166-2525. DOI: 10.1137/15M1050239.
- Lobsien, Jim-Felix et al. “Improved performance of stellarator coil design optimization”. In: *Journal of Plasma Physics* 86.2 (Apr. 2020). DOI: 10.1017/S0022377820000227.
- Lobsien, Jim-Felix et al. “Physics analysis of results of stochastic and classic stellarator coil optimization”. In: *Nuclear Fusion* 60.4 (Apr. 2020). DOI: 10.1088/1741-4326/ab7211.

- Lobsien, Jim-Felix et al. “Stellarator coil optimization towards higher engineering tolerances”. In: *Nuclear Fusion* 58.10 (Oct. 2018). DOI: 10.1088/1741-4326/aad431.
- Neilson, G. H. et al. “Lessons Learned in Risk Management on NCSX”. In: *IEEE Transactions on Plasma Science* 38.3 (2010), pp. 320–327.
- Paul, E.J. et al. “An adjoint method for gradient-based optimization of stellarator coil shapes”. In: *Nuclear Fusion* 58.7 (May 2018), p. 076015. DOI: 10.1088/1741-4326/aac1c7.
- Pedersen, T. Sunn et al. “Experimental demonstration of a compact stellarator magnetic trap using four circular coils”. In: *Physics of Plasmas* 13.1 (Jan. 2006). ISSN: 1070-664X, 1089-7674. DOI: 10.1063/1.2149313.
- Rasmussen, Carl Edward and Christopher K. I. Williams. *Gaussian processes for machine learning*. Adaptive computation and machine learning. Cambridge, Mass: MIT Press, 2006.
- Rasmussen, CE. and CKI. Williams. *Gaussian Processes for Machine Learning*. Adaptive Computation and Machine Learning. Cambridge, MA, USA: MIT Press, Jan. 2006, p. 248.
- Rockafellar, R. Tyrrell and Stanislav Uryasev. “Optimization of conditional value-at-risk”. en. In: *The Journal of Risk* 2.3 (2000), pp. 21–41. ISSN: 14651211. DOI: 10.21314/JOR.2000.038.
- Rummel, T. et al. “Accuracy of the Construction of the Superconducting Coils for WENDELSTEIN 7-X”. en. In: *IEEE Transactions on Applied Superconductivity* 14.2 (June 2004), pp. 1394–1398. ISSN: 1051-8223. DOI: 10.1109/TASC.2004.830584.
- Schölkopf, Bernhard and Alexander J. Smola. *Learning with kernels: support vector machines, regularization, optimization, and beyond*. Adaptive computation and machine learning. Cambridge, Mass: MIT Press, 2002.
- Shapiro, Alexander, Darinka Dentcheva, and Andrezj Ruszczyński. *Lectures on Stochastic Programming: Modeling and Theory*. Society for Industrial and Applied Mathematics, 2009.
- Strickler, Dennis J., Lee A. Berry, and Steven P. Hirshman. “Designing Coils for Compact Stellarators”. In: *Fusion Science and Technology* 41.2 (Mar. 2002), pp. 107–115. DOI: 10.13182/FST02-A206.
- Strykowski, R. L. et al. “Engineering cost schedule lessons learned on NCSX”. In: *2009 23rd IEEE/NPSS Symposium on Fusion Engineering*. 2009, pp. 1–4.
- Virtanen, Pauli et al. “SciPy 1.0: fundamental algorithms for scientific computing in Python”. In: *Nature Methods* 17.3 (2020), pp. 261–272.
- Wang, Qiqi et al. “Conditional sampling and experiment design for quantifying manufacturing error of transonic airfoil”. In: *49th AIAA Aerospace Sciences Meeting including the New Horizons Forum and Aerospace Exposition*. Orlando, Florida: American Institute of Aeronautics and Astronautics, Jan. 2011. ISBN: 978-1-60086-950-1. DOI: 10.2514/6.2011-658.
- Zhu, Caoxiang et al. “Designing stellarator coils by a modified Newton method using FOCUS”. In: *Plasma Physics and Controlled Fusion* 60.6 (Apr. 2018), p. 065008. DOI: 10.1088/1361-6587/aab8c2.
- Zhu, Caoxiang et al. “Hessian matrix approach for determining error field sensitivity to coil deviations”. In: *Plasma Physics and Controlled Fusion* 60.5 (Apr. 2018), p. 054016. DOI: 10.1088/1361-6587/aab6cb.

- Zhu, Caoxiang et al. “Identification of important error fields in stellarators using the Hessian matrix method”. In: *Nuclear Fusion* 59.12 (Sept. 2019), p. 126007. DOI: 10.1088/1741-4326/ab3a7c.
- Zhu, Caoxiang et al. “New method to design stellarator coils without the winding surface”. In: *Nuclear Fusion* 58.1 (Jan. 2018), p. 016008. ISSN: 0029-5515, 1741-4326. DOI: 10.1088/1741-4326/aa8e0a.